Sex-specific mechanisms of cerebral microvascular BK_{Ca} dysfunction in a mouse model of Alzheimer's disease.

Josiane F. Silva[1], Felipe D. Polk[1,*], Paige E. Martin[1,*], Stephenie H. Thai[1], Andrea Savu[1], Matthew Gonzales[1], Allison M. Kath[1], Michael T. Gee[1], Paulo W. Pires[1,2,3,#]

[1]Department of Physiology, [2]Sarver Heart Center, [3]Bio5 Institute, University of Arizona College of Medicine, Tucson, AZ, 85721, USA.

[*]Equal contribution

[#]Corresponding Author

Running title: Sex-dependent neurovascular dysfunction in *5x-FAD*

Address for Correspondence: Paulo W. Pires, Ph.D.
1656 E Mabel St, Room 426
Medical Research Building
Tucson, AZ 85721
PO Box 245051
Phone: +1 (520) 626-8632
Email: ppires@arizona.edu

Keywords: cerebral pial arteries, BK_{Ca} channels, nitrosylation, cerebral functional hyperemia, Ca^{+2} sparks, sex as a biological variable

Abstract

Background: Cerebral microvascular dysfunction and nitro-oxidative stress are present in patients with Alzheimer's disease (AD) and may contribute to disease progression and severity. Large conductance Ca^{2+}-activated K^+ channels (BK_{Ca}) play an essential role in vasodilatory responses and maintenance of myogenic tone in resistance arteries. BK_{Ca} impairment can lead to microvascular dysfunction and hemodynamic deficits in the brain. We hypothesized that reduced BK_{Ca} function in cerebral arteries mediates microvascular and neurovascular responses in the *5x-FAD* model of AD. *Methods:* BK_{Ca} activity in the cerebral microcirculation was assessed by patch clamp electrophysiology and pressure myography, in situ Ca^{2+} sparks by spinning disk confocal microscopy, hemodynamics by laser speckle contrast imaging. Molecular and biochemical analyses were conducted by affinity-purification assays, qPCR, Western blots and immunofluorescence. *Results:* We observed that pial arteries from 5-6 months-old male and female *5x-FAD* mice exhibited a hyper-contractile phenotype than wild-type (WT) littermates, which was linked to lower vascular BK_{Ca} activity and reduced open probability. In males, BK_{Ca} dysfunction is likely a consequence of an observed lower expression of the pore-forming subunit BK_{α} and blunted frequency of Ca^{2+} sparks, which are required for BK_{Ca} activity. However, in females, impaired BK_{Ca} function is, in part, a consequence of reversible nitro-oxidative changes in the BK_{α} subunit, which reduces its open probability and regulation of vascular tone. We further show that BK_{Ca} function is involved in neurovascular coupling in mice, and its dysfunction is linked to neurovascular dysfunction in the model. *Conclusion:* These data highlight the central role played by BK_{Ca} in cerebral microvascular and neurovascular regulation, as well as sex-dependent mechanisms underlying its dysfunction in a mouse model of AD.

Introduction

Alzheimer's disease (AD) is a neurodegenerative disorder associated with global cognitive decline that affects more than 6 million people in the United States alone[1,2], and approximately 2/3 of all AD cases are women[1,3]. Alarmingly, it is projected that more than 130 million people will live with AD worldwide by 2050[1,3]. One of the hallmarks of AD is cerebral amyloid angiopathy (CAA), characterized by perivascular accumulation of amyloid-β, which is present in more than 80% of all AD patients[4]. This accumulation is proposed to induce microvascular fragility, contributing to the development of intracerebral hemorrhages[5], loss of blood-brain-barrier integrity [6], and blood flow deficits[7]. These deficits may be a consequence of microvascular dysfunction, which impairs cerebrovascular reserve and neurovascular coupling[8], a vital process that matches local hyperemia to increased neuronal activity[9]. The ability of the cerebral microcirculation to accommodate these second-to-second changes in local perfusion depends on two main phenomena: the extent of myogenic tone (the intrinsic contractile property of vascular smooth muscle cells that stipulates the vasodilatory reserve) and mechanisms underlying vasorelaxation. Both mechanisms are dependent on the membrane potential of smooth muscle cells: depolarization favors constriction, whereas hyperpolarization favors dilation. Thus, regulation of ion flux is paramount for microvascular function, particularly modulation of K^+ permeability, of which the large-conductance Ca^{2+}-activated K^+ channel (BK_{Ca}) is central.

BK_{Ca} are widely expressed channels that play a critical role in regulating arterial tone by conducting hyperpolarizing currents in vascular smooth cells to oppose vasoconstriction[10,11]. Opening of BK_{Ca} channels occurs downstream from localized intracellular Ca^{2+} release from ryanodine receptors located in the sarcoplasmic reticulum (Ca^{2+} sparks), which activates BK_{Ca} channels, leading to hyperpolarization and dilation[10,12]. BK_{Ca} channels are composed of two subunits, a selective pore (BK_{α}) and regulatory ($BK_{\beta1}$, BK_{γ}) subunits[13]. Further, BK_{Ca} undergoes extensive pre- and post-translational modifications (PTM), including phosphorylation[14-16], oxidation and nitrosylation, all affecting channel open probability (Po) and conductance[16]. In some tissues, oxidation increases channel activity[17,18], whereas, in others, it markedly inhibits BK_{Ca}[19-21]. Similarly, nitrosylation of thiol moieties due to an electrophilic attack by peroxynitrite, formed by a reaction between nitric oxide (NO) and superoxide (O_2^-) in a pro-oxidative environment[22-24], as seen in AD[25-27], inhibits BK_{Ca} currents[19]. Despite recent evidence of BK_{Ca} impairment in male APP23 mice[28], it remains unknown if the reduction in cerebral microvascular BK_{Ca} occurs in females *via* similar mechanisms, and whether neurovascular dysfunction accompanies loss of BK_{Ca} activity. Using a combination of molecular and biochemical tools, ex vivo patch clamp

electrophysiology and microvascular pressure myography, and *in vivo* hemodynamic assessments, we show that BK_{Ca} dysfunction mediates cerebral microvascular and neurovascular dysfunction in in both males and females *5x-FAD*. Remarkably, the mechanisms underlying this dysfunction show sex-specificity: In males, we observed lower BK_{α} expression and reduced Ca^{2+} sparks frequency; however, in females, there is an exacerbated and partially reversible nitro-oxidative modification of BK_{α}.

Methods

All animal procedures in this study were approved by the Institutional Animal Care and Use Committee of the University of Arizona College of Medicine (IACUC protocol 18-473) and are in accordance with the National Institutes of Health's Guide for the Care and Use of Laboratory Animals, 8th edition. All animal experiments are reported in compliance with ARRIVE guidelines. The *5x-FAD* mice (5-6 months-old) used in this study are a transgenic model of early-onset AD that combines five different mutations in two genes associated with Familial AD. Three of the mutations are located in the gene that codes human amyloid precursor protein: Swedish (K670N, M671L), Florida (I716V), and London (V717I). The other two mutations are inserted in the gene of human presenilin, M146L and L286V. Transgene expression is controlled by the neuronal-specific *Thy1* promoter[29]. All mice were bred on a C57bl/6J background, and wild-type (WT) littermates were used as controls. Following euthanasia, the brain was collected and the pial arteries were dissected for patch clamp electrophysiology, pressure myography and quantification of vascular smooth muscle cells Ca^{2+} sparks activity by spinning disk confocal microscopy. The brain was either fixed in 4% paraformaldehyde for immunofluorescence, or flash-frozen for molecular biology and biochemical experiments (oxidized glutathione assay, affinity-purification of nitrosylated proteins followed by Western blot and qPCR). Baseline cortical perfusion and functional hyperemia following somatosensory stimulation were measured by laser speckle contrasting imaging.

Post-mortem brain tissues from CAA / AD and age-matched controls (no CAA or AD diagnosed) were used for assessment of BK_{α} S-NO by affinity-purification followed by Western blot. All human samples were kindly donated by the Brain and Body Donation Program from Banner Health, and are in compliance with all guidelines and requirements for patient de-identification. The complete and detailed methodology can be found in the *Supplemental Information - Methods.*

122 **Results**

123 ***Amyloid-β accumulation is higher in female 5x-FAD mice***

124 One of the hallmarks of Alzheimer's disease is the accumulation of amyloid-β peptides in
125 the brain and cerebral microvasculature[30]. In this study, *5x-FAD* female mice showed a trend
126 towards higher density of amyloid-β plaques in the cortex and hippocampus when compared with
127 age-matched male *5x-FAD* (Figures S1A and S1B). No significant perivascular amyloid-β
128 accumulation was observed in the parenchymal microcirculation of male or female *5x-FAD* mice
129 (Figures S1C and S1D). We previously showed that pial arteries in this model exhibit extensive
130 amyloid-β accumulation[31]. However, in our previous publication, we did not separate the incidence
131 of pial vessel CAA by sex. Thus, we reanalyzed those data and observed no sex differences in
132 pial vessel CAA in *5x-FAD* mice (Figures S1E, and S1F). Given the lack of microvascular
133 intraparenchymal CAA in *5x-FAD*, we focused our vascular reactivity studies on the pial
134 microcirculation.

135

136 ***Increased contractility of pial arteries in 5x-FAD mice.***

137 Along with amyloid-β plaque accumulation, microvascular dysfunction is implicated in AD
138 pathophysiology[30]. We observed an exacerbated contractile response in pial arteries of both
139 female and male *5x-FAD* when compared to wild-type (WT) littermates, shown as higher
140 spontaneous myogenic tone at a purported physiological intraluminal pressure compared to the
141 respectively WT (50 mmHg, Figures 1A-B and 1E-F). Similarly, contractile response to a receptor-
142 dependent stimulus (endothelin-1 [ET-1], 30 nM, Figures 1C and 1G) was higher in females and
143 males *5x-FAD* mice than WT. No differences were observed in contractile responses to a
144 receptor-independent depolarizing stimulus (60 mM $[K^+]_E$, Figures 1D and 1H). Thus, we conclude
145 that contractile responses to a steady intraluminal pressure, as well as receptor-induced, are
146 exacerbated in pial arteries of *5x-FAD* mice.

147 We then characterized autoregulatory responses (myogenic reactivity) of pial arteries in
148 *5x-FAD* and WT littermates by step-wise increases in intraluminal pressure (from 5 mmHg to 160
149 mmHg). Under our experimental conditions, myogenic reactivity was not altered in *5x-FAD*, both
150 females and males (Figure S2). Similarly, pial arteries from female or male *5x-FAD* do not undergo
151 significant structural remodeling (Figure S3) or alterations in biomechanical properties (Figure

152 S4). Thus, the enhanced contractility of pial arteries observed is independent of microvascular
153 remodeling.

154

155 ***Reduced BK_{Ca} channel function in pial arteries from 5x-FAD***

156 BK_{Ca} channel is an important mechanism that provides negative feedback to myogenic
157 constriction[32]. Therefore, to test whether the increased contractility observed in *5x-FAD* was due
158 to BK_{Ca} dysfunction, we incubated pial arteries with the BK_{Ca} channel blocker iberiotoxin (IbTox,
159 30 nM). IbTox-induced vasoconstriction was significantly smaller in pial arteries isolated from *5x-*
160 *FAD* when compared to WT littermates, for both females and males (Figures 2A-B and 2E-F),
161 suggesting impaired BK_{Ca} activity in *5x-FAD* mice.

162 We next corroborated the pressure myography findings by recording pial artery smooth
163 muscle cell single channel BK_{Ca} currents in excised, inside-out patch-clamp electrophysiology
164 experiments. We observed an approximately 50% lower BK_{Ca} open probability (Po) at +60 mV in
165 patches from *5x-FAD* female than those from WT littermates (Figures 2C and 2D). However, in
166 males, BK_{Ca} Po was not significantly different between WT and *5x-FAD* (Figures 2G and 2H).

167 Interestingly, when comparing IbTox constriction between WT females and males, we
168 observed a significantly smaller constriction in pial arteries of males than in females
169 (Vasoconstriction (%): 10.6 ± 1.2 vs 6.6 ± 1.3, WT females vs WT males, $p = 0.0494$, two-tailed
170 *Student*'s t-test). This finding was again corroborated by patch-clamp electrophysiology: BK_{Ca} Po
171 was significantly lower in WT males when compared to females (BK_{Ca} Po at +60 mV: 0.118 ±
172 0.025 vs 0.040 ± 0.013, WT females vs WT males, $p = 0.0125$, two-tailed *Student*'s t-test). These
173 data suggest that physiological BK_{Ca} activity is lower in pial artery smooth muscle cells from males
174 than in female WT mice.

175

176 ***5x-FAD males, but not females, have lower BK_{α} expression in pial arteries***

177 To investigate if the reduced constriction to IbTox in *5x-FAD* mice was due to lower
178 expression of BK_{Ca}, we assessed mRNA expression of BK_{α} and $BK_{\beta 1}$ subunits in lysates of pial
179 arteries from female and male *5x-FAD* and WT littermates by qPCR. Pial artery mRNA expression
180 of both subunits was not significantly different between *5x-FAD* and WT in females (Figures 3A
181 and S5A) or males (Figures 3C and S5B). Using Western blot, we then measured expression of
182 the BK_{α} protein in pial artery lysates, and observed that, in females, expression of BK_{α} was similar

183 between WT and *5x-FAD* (Figure 3B). However, expression of BK_{α} protein was significantly lower
184 in male *5x-FAD* when compared to WT littermates (Figure 3D). An image of the membrane used
185 for the inserts can be found in Figure S6.

186 In brain lysates, we observed a downregulation of BK_{α} mRNA in female *5x-FAD* when
187 compared to WT littermates (Figure S5C), without changes in mRNA for $BK_{\beta 1}$ (Figure S5D). No
188 significant differences were observed in mRNA for BK_{α} and $BK_{\beta 1}$ in brain lysates from male *5x-*
189 *FAD* when compared to WT (Figures S5E and S5F).

190

191 ***Lower frequency of Ca^{2+} sparks in pial arteries from male 5x-FAD mice, but not in females***

192 We next investigate whether the observed BK_{Ca} dysfunction was downstream from
193 alterations in intracellular Ca^{2+} sparks, as shown previously in male APP23 mice[28]. Our data show
194 that Ca^{2+} sparks frequency is significantly higher in pial artery smooth muscle cells of female *5x-*
195 *FAD* mice than WT littermates (Figure 3I, Movies S1 and S2), without changes in the number of
196 Ca^{2+} sparks sites per cell (Figures 3E, 3F and 3J). In contrast, Ca^{2+} spark frequency was
197 significantly lower in pial artery smooth muscle cells of male *5x-FAD* than in WT (Figure 3K,
198 Movies S3 and S4). This reduction was not due to a lower number of active Ca^{2+} sparks site per
199 cell, as these were not different between males *5x-FAD* and WT (Figures 3G, 3H and 3L).
200 Altogether, our findings show that BK_{Ca} dysfunction in *5x-FAD* male is due to lower expression of
201 BK_{α} and reduced Ca^{2+} sparks frequency, whereas in females we observed an increase in Ca^{2+}
202 sparks frequency without changes in BK_{α} expression.

203

204 ***Oxidative stress impairs BK_{Ca} in female 5x-FAD***

205 AD is associated with oxidative stress and inflammation that can contribute to vascular
206 and neuronal damage[26,33]. Thus, we investigated if oxidative stress was present in the brain of
207 *5x-FAD* using an oxidized glutathione assay. We observed that, in females, total glutathione (Total
208 GSH) levels were similar between WT and *5x-FAD* (Figure 4A). However, brain levels of oxidized
209 glutathione (GSSG, Figure 4B) and the ratio GSSG / Total GSH (Figure 4C) were significantly
210 higher in female *5x-FAD* than WT littermates, suggesting the presence of an oxidative
211 environment. None of the assessed parameters were altered in male *5x-FAD* when compared to
212 WT littermates (Figure S7A-S7C).

213 We then hypothesized that this oxidant environment leads to reversible PTM in pial artery
214 BK_{Ca} in female *5x-FAD*, thus causing its impairment. We tested this hypothesis by incubating *ex*
215 *vivo* pial arteries and excised inside-out membrane patches with the broad-spectrum reducing
216 agent dithiothreitol (DTT, 10 μM). We observed that DTT partially reversed pial artery sensitivity
217 to IbTox in females, observed as a larger vasoconstriction response after incubation with DTT
218 (Figures 4D and 4E). These findings were corroborated in patch-clamp electrophysiology
219 experiments, as incubation of patches with DTT partially restored BK_{Ca} Po (Figures 4F and 4G).
220 DTT did not affect BK_{Ca} Po in pial artery smooth muscle cells isolated from male *5x-FAD* (Figure
221 S7D-S7E). Altogether, these data suggest that the oxidative environment in female, but not males,
222 *5x-FAD* leads to oxidation of BK_{Ca}, consequently reducing its function in pial artery smooth muscle
223 cells.

224

225 ***Exacerbated BK_{Ca} S-nitrosylation in female 5x-FAD and CAA / AD patients***

226 Next, we sought to identify the likely type of PTM responsible for the observed BK_{Ca}
227 impairment. The inducible nitric oxide synthase (iNOS) isoform is a pro-inflammatory enzyme that
228 is increased in the AD brain[34,35]. This isoform produces a high amount of NO, which can lead to
229 nitro-oxidative damage of cellular structures[36,37], including excessive nitrosylation of target
230 proteins. Thus, we investigated if iNOS expression is increased in the pial arteries of *5x-FAD*
231 females. Using qPCR, we observed that the expression of iNOS mRNA was increased in the pial
232 arteries from female *5x-FAD* mice compared to WT (Figure 5A). No significant differences were
233 observed for endothelial (eNOS, Figure S8A) or neuronal NOS (nNOS, Figure S8B) in pial
234 arteries. To corroborate the mRNA findings, we performed a semi-quantitative assessment of
235 fluorescence intensity of iNOS immunolabeling in pial arteries, which was significantly higher in
236 pial vessels from female *5x-FAD* than in WT mice (Figures 5B and 5C). These results suggest
237 that iNOS is upregulated on the pial vessels from female, but not male, *5x-FAD* mice. Lastly,
238 inhibition of NOS with L-NAME (200 μM) induced a greater pial artery constriction in *5x-FAD* than
239 in WT littermates (Figure S8C).

240 Excessive NO production in the presence of an oxidative environment can lead to
241 excessive protein S-NO[38], thus we investigated if this particular PTM was involved in the BK_{Ca}
242 dysfunction observed in female *5x-FAD*. Our findings show that total S-NO proteins were
243 significantly higher in brain lysates of female *5x-FAD* when compared to WT littermates (Figures
244 5D-5E), but not in male *5x-FAD*, where they were actually significantly reduced (Figure S9). We

245 then performed an affinity-purification of S-NO proteins from brain lysates of female *5x-FAD* and
246 WT littermates, followed by Western blot against the BK_α subunit. We observed a significant
247 increase in the amount of BK_α S-NO (Figures 5F-G, whole blot of inserts in Figure S10). We
248 corroborated these findings by performing a co-immuno-localization assay to investigate
249 vascular-specific BK_α S- NO (Figure 5H). Our data shows that there is a significant increase in
250 co-localization between the BK_α subunit and S-NO proteins, as evidenced by the M1 / M2 –
251 Mander's coefficients (Figures 5I-5J) and the Pearson's coefficient (Figure 5K). Together, these
252 findings support our hypothesis that the pro-nitro-oxidative environment in *5x-FAD* females leads
253 to excessive BK_α S-NO.

254 We then investigated if the increase in BK_α S-NO observed in *5x-FAD* was also present in
255 humans with CAA or AD. We obtained post-mortem brain samples from the Banner Brain and
256 Body Donation Program, from age-matched women and men, and separated them in 3 groups:
257 healthy (non-CAA / non-ADA, n=6), CAA / non-AD (CAA, n=6) and AD + CAA (n=12). Healthy
258 patients were defined no presence of dementia or symptoms of parkinsonism, and no presence
259 of CAA or senile plaques in histopathology. CAA / non-AD were patients without dementia or
260 parkinsonism, but with evident perivascular amyloid plaques and no presence of senile plaques.
261 AD + CAA were patients with Alzheimer's disease with a minimum of intermediate or high NIA-
262 Reagan criteria[39], and presence of CAA and / or senile plaques. Using Western blot, we observed
263 that there was a trend towards an increase in BK_α subunit expression in brain from AD + CAA
264 patients (p=0.0976, Brown-Forsythe and Welch's ANOVA), without evident sex differences
265 (Figures 6A-6B). When performing an affinity purification of S-NO proteins followed by Western
266 blot, we again observed a trend towards an increase in BK_α S-NO in AD + CAA patients
267 (p=0.0772, Brown-Forsythe and Welch's ANOVA), without sex differences (Figures 6C-6D).
268 Images of the whole blots shown in the cropped insets (Figures 6A and 6C) can be found in the
269 Figure S11. These findings suggest that BK_α S-NO is also present in AD patients, although in
270 both women and men.

271

272 ***Cerebral perfusion deficits in female 5x-FAD***

273 Next, we investigated if there are changes in basal cortical perfusion in *5x-FAD* females
274 and males compared to sex-matched WT littermates. Using laser speckle contrast imaging, we
275 observed that the baseline perfusion of the entire superficial cortex was not different between WT
276 and *5x-FAD* females (Figures S12B-S12C, WC: whole cortex**)** or males (Figures S12D-S12E**,**

277 WC: whole cortex). However, when analyzing discrete perfusion of specific vascular territories
278 (diagram in Figures S12A)[40], we observed that *5x-FAD* females showed lower basal perfusion to
279 the frontal cortex (Figures S12B-S12C), but not in other regions. No significant differences were
280 observed in cortical perfusion of male *5x-FAD* mice (Figures S12D-S12E).

281

282 ***Impaired functional neurovascular responses in females and males 5x-FAD***

283 We next tested the hypothesis that impaired vascular BK_{Ca} would result in neurovascular
284 dysfunction in *5x-FAD*. First, we showed that acutely inhibiting BK_{Ca}, achieved by applying IbTox
285 (30 nM) atop the thinned-skull cranial window, significantly blunted hyperemic responses on the
286 somatosensory cortex during mechanical stimulation of contralateral whiskers[41] (Figures 7A-7C),
287 suggesting that BK_{Ca} play a role in neurovascular responses. We then assessed neurovascular
288 responses in *5x-FAD* mice and compared to WT littermates. We observed that both females
289 (Figures 7D-7F) and males (Figures 7G-7I) *5x-FAD* had significantly lower hyperemic responses
290 than WT littermates. Together, these findings suggest that the cerebral vascular impairment
291 observed in *5x-FAD* mediates neurovascular dysfunction in the model.

292

293 **Discussion**

294 Our findings show that cerebral BK_{Ca} microvascular dysfunction is present in both female
295 and male *5x-FAD*, likely mediating neurovascular impairments in the model. A major novelty of
296 our study lies in our findings elucidating the distinct mechanisms underlying BK_{Ca} dysfunction in
297 females and males. In males, we observed reduced expression of the BK_{α} subunit and lower Ca^{2+}
298 sparks frequency. On the other hand, in females, we show that BK_{α} expression is unchanged and
299 Ca^{2+} sparks frequency is higher, yet BK_{Ca} activity is likewise impaired. Upon further investigation,
300 we uncovered that the BK_{α} subunit in female *5x-FAD* undergoes oxidative modification,
301 particularly excessive S-NO, and this partially underlies cerebral microvascular BK_{Ca} dysfunction.
302 The exacerbation in nitrosylation is downstream from increased vascular iNOS expression and
303 general oxidative stress in the brain environment, none of which were present in males (Figure
304 S13). Lastly, we describe two other novel findings in our study: basal cerebral microvascular BK_{Ca}
305 activity seems lower in male than in female C57Bl/6J mice, and that BK_{Ca} function is involved in
306 physiological neurovascular responses, as its blockade blunts somatosensory-induced functional
307 hyperemia. Altogether, our data highlight the complexities of microvascular regulation in the

308 context of AD, and the differential effects of biological sex that may hinder putative therapies
309 ineffective as a “one size fits all” approach.

310 AD is a progressive neurodegenerative disease characterized by accumulation of amyloid-
311 β and neurofibrillary tangles, particularly in the temporal lobe and neocortical structures[42], which
312 lead to cognitive deficits[30]. Beyond misfolded protein pathology, cerebral vascular dysfunction
313 contributes to AD progression, and much attention has been placed on loss of endothelial function
314 and blood-brain-barrier breakdown[43,44]. However, less is known on how cerebral microvascular
315 smooth muscle cell function is affected in AD, as well as its participation in AD’s development and
316 progression. A recent report by Taylor *et al.* described that acute exposure of cerebral arteries
317 isolated from male C57Bl/6 mice to amyloid-$\beta_{(1\text{-}40)}$ increases myogenic tone due to impaired BK_{Ca}
318 activity[28]. Our findings expand on this report, and we show that not only spontaneous myogenic
319 tone is higher in *5x-FAD*, a mouse model of AD with accumulation of both amyloid-$\beta_{(1\text{-}40)}$ and
320 amyloid-$\beta_{(1\text{-}42)}$ (predominant), but so is contractility to ET-1. These data suggest the presence of
321 a general hyper-contractile state in the cerebral microcirculation in both female and male arteries
322 during AD progression. Our data suggests that BK_{Ca} impairment likely underlies this hyper-
323 contractile status in *5x-FAD*, as its function is impaired in *ex vivo* pressurized arteries.
324 Paradoxically, we did not observe any significant changes in autoregulation. Although loss of
325 autoregulation is observed in cerebral small vessel disease[45] and it was shown to occur in some
326 rodent models of AD[46], human studies have also failed to observe cerebral autoregulation
327 impairments in AD patients[47]. The mechanistic explanation underlying these differences in
328 autoregulation between AD models and humans remain unclear and require further exploration.

329 Impairment in BK_{Ca} function is associated with vascular dysfunction in various disease
330 models, including diabetes[48,49], hypertension[50,51], menopause[41,52], cigarette smoking[53] and AD[28].
331 One limitation of the aforementioned studies is that they were all performed in a single sex, and
332 the vast majority in males (with the exception of studies focused on menopause). Our findings
333 expand on these previous observations and show a sex-dependent mechanism of BK_{Ca}
334 impairment in *5x-FAD*. We show that BK_{Ca} activity is reduced in pial arteries independently of
335 biological sex, observed as blunted constriction to iberiotoxin. However, the cellular and molecular
336 mechanisms responsible for the lower BK_{C}a activity diverge between females and males. We
337 observed that, in male *5x-FAD*, single channel BK_{Ca} Po was not lower than that recorded from
338 WT littermates, indicating that BK_{Ca} dysfunction was likely upstream from intracellular signals
339 regulating BK_{Ca} activity. Upon further investigation, we describe that expression of the pore-
340 forming subunit BK_{α} is lower in male *5x-FAD* than in WT littermates, which could account for lower

341 sensitivity to Iberiotoxin in pressure myography experiments. In addition, frequency of Ca^{2+} sparks
342 was significantly reduced in male *5x-FAD*, similar to data published by Taylor *et al.* in male APP23
343 mice[28]. On the other hand, female *5x-FAD* showed reduced single channel BK_{Ca} Po despite
344 similar levels of BK_{α} expression and an increase in Ca^{2+} spark frequency, suggesting that, in
345 females, BK_{Ca} dysfunction was likely due to molecular alterations in the BK_{α} subunit itself, such
346 as PTMs resulting from nitro-oxidative stress.

347 In support of this hypothesis, we observed that brains of females *5x-FAD*, but not males,
348 show an increase in markers of oxidative and nitrosative stress, observed as higher levels of
349 oxidized glutathione (GSSG) and higher levels of global S-NO proteins. Together, this nitro-
350 oxidative environment can result in exacerbated PTMs within the BK_{α} subunit. PTMs are the result
351 of binding of different moieties to proteins, such as phosphorylation, acetylation, lipidation,
352 oxidation and nitrosylation[24,54]. PTMs play a vital role in the known heterogeneity and tissue
353 specificity of the biophysical properties of BK_{Ca}, as they have profound effects on gating, voltage
354 and Ca^{2+} sensitivity, and membrane availability of the channel[16]. However, how S-NO affects BK_{Ca}
355 remains controversial: some studies show that NO can, directly or indirectly, activate BK_{Ca}[55,56],
356 whereas others show that NO itself, or peroxynitrite, do not affect or can blunt BK_{Ca} activity. For
357 instance, a NO-donor failed to activate the BK_{Ca} channel in a heterologous expression system[57].
358 Moreover, Liu *et al.* showed that peroxynitrite reduces the open-state probability of BK_{Ca} channels
359 in isolated vascular smooth muscle cells[58]. We show that, in female *5x-FAD*, the BK_{α} subunit
360 undergoes excessive S-NO, and this nitro-oxidative PTM likely mediates channel dysfunction in
361 a reversible manner. This assertion is supported by our data that the broad-spectrum reducing
362 agent DTT partially recover single BK_{Ca} Po and arterial responsiveness to iberiotoxin. Although
363 the molecular mechanisms of how S-NO impair BK_{Ca} remain undetermined, we speculate that
364 they may reduce Ca^{2+} sensitivity of the BK_{α} subunit, which may explain the increase in Ca^{2+} sparks
365 frequency observed in female *5x-FAD*, likely to compensate for such lower sensitivity. This,
366 however, remains untested.

367 We further made efforts to elucidate the cellular source responsible for excessive protein
368 S-NO, and observed an increase in cerebral vascular iNOS expression. Inducible NOS (NOS2)
369 is commonly upregulated under stress and inflammatory conditions[34], such as is observed in AD
370 and other dementias[33,59]. Distinctly from the other NOS isoforms (eNOS and nNOS), iNOS is
371 effectively locked in an active position due to the tight binding of calmodulin[34,60], leading to
372 sustained basal NO production. Together with oxidative stress, the higher NO production can
373 result in excessive protein S-NO, as we observed in female *5x-FAD*. Further, we observed a trend

374 towards an increase in BK_{α} S-NO in *post-mortem* brain samples from patients with AD + CAA
375 when compared to age-matched non-dementia controls (healthy), without any evident changes in
376 BK_{α} expression. Interestingly, in humans, our data does not indicate the presence of sex
377 differences, as both women and men show BK_{α} S-NO. The discrepancies between the human
378 and *5x-FAD* findings are not immediately apparent, but we speculate that other co-morbidities in
379 males may increase BK_{α} S-NO in men, including cigarette smoking or cardiovascular disease.
380 We currently do not have the medical records of the patients included in our samples; therefore,
381 this possibility remains a speculation.

382 Ultimately, our observed microvascular BK_{Ca} dysfunction may underlie the functional
383 perfusion deficits observed in *5x-FAD*. We show that acute application of iberiotoxin atop the
384 cranial window blunts neurovascular responses in both female and male C57Bl/6J mice, showing
385 the role of BK_{Ca} in these functional hemodynamic responses, as shown by others using an *ex vivo*
386 brain slice preparations[61]. Further, both females and males *5x-FAD* mice showed a reduction in
387 neurovascular responses during somatosensory stimulation. A similar neurovascular impairment
388 was recently reported by us, in which female mice that underwent chemically-induced menopause
389 showed reduced functional hyperemia responses associated with cerebral microvascular BK_{Ca}
390 impairment[41]. However, it is important to note that these studies, and our data presented herein,
391 are associative, and further experiments are needed to definitively show the role of cerebral
392 microvascular BK_{Ca} in neurovascular coupling responses. Regardless, our previous and current
393 findings, in conjunction with findings from others[28,51,62], reiterate the central role played by BK_{Ca} in
394 basal physiological hemodynamic regulation in the brain, as well as its importance in
395 cerebrovascular diseases.

396 Lastly, the molecular basis of the sex differences observed remains unclear. Sex
397 differences are commonly reported in mouse models of AD[63,64], as well as in humans, and sex
398 hormones seem to play a role. Female *5x-FAD* and AD patients have lower expression of
399 aromatase in the hippocampus, an important enzyme that produces 17β-estradiol[65]. Since
400 estradiol can play a role in vascular function[66,67], neuroplasticity[68], synaptic stability[68], as well as
401 attenuation of oxidative stress[69], it is possible that reduction in its concentration or bioavailability
402 may result underlie the heightened AD pathology in females. Further, in *5x-FAD* mice harboring
403 human ApoE3 or ApoE4, ovariectomy worsens cognitive function, and β-estradiol partially
404 recovers cognition in *5x-FAD* x ApoE3, with little effect in *5x-FAD* x ApoE4. Testes levels of
405 testosterone are higher in male *5x-FAD* than in wild-type, without changes in sperm viability,

406 testosterone levels are higher[70]. Currently, there are no published studies showing the effects of
407 castration on *5x-FAD* males.

408 In conclusion, our results show that the BK_{Ca}-dependent microvascular and neurovascular
409 dysfunction occurs in both male and female *5x-FAD*, although the mechanisms underlying BK_{Ca}
410 impairment differ based on biological sex. Further, we show that one of such mechanisms, namely
411 excessive BK_{α} S-NO, may also be present in humans with AD and CAA, suggesting that
412 manipulation of this basic pathophysiological mechanism could have therapeutic potential.

413

414 **Novelty and Significance**

415 Cerebrovascular dysfunction is a hallmark of Alzheimer's disease and related dementias.
416 A property of the resistance vasculature is to constrict when pressurized (myogenic tone);
417 however, over-constriction can be detrimental. Feedback mechanisms, including the opening of
418 BK_{Ca}, exist to keep the system in balance. Here, using a combination of molecular biology with *ex*
419 *vivo* and *in vivo* assessments, we show a novel mechanism associated with BK_{Ca} dysfunction in
420 the cerebral microvasculature of female *5x-FAD* mice. We report increased BK_{Ca} S-nitrosylation
421 linked to higher myogenic tone and reduced channel activity. These changes were associated
422 with lower perfusion of the frontal cortex and impaired neurovascular reactivity, suggesting that
423 nitro-oxidative stress is an important mechanism of vascular dysfunction in Alzheimer's disease
424 in mice and human.

425

426 **Acknowledgments**

427 We thank Patricia Jansma, co-manager of the Office Research, Innovation & Impact's
428 Imaging Cores - Optical Facility at the University of Arizona, for providing training service at the
429 microscope and helping with the microscopy image acquisition. We would further like to thank Dr.
430 Anne M. Dorrance (Michigan State University) for her critical review of our manuscript.

431 We are grateful to the Banner Sun Health Research Institute Brain and Body Donation
432 Program of Sun City, Arizona for the provision of human biological materials. The Brain and Body
433 Donation Program has been supported by the National Institute of Neurological Disorders and
434 Stroke (U24 NS072026 National Brain and Tissue Resource for Parkinson's Disease and Related
435 Disorders), the National Institute on Aging (P30 AG19610 and P30AG072980, Arizona
436 Alzheimer's Disease Center) the Arizona Department of Health Services (contract 211002,

Arizona Alzheimer's Research Center), the Arizona Biomedical Research Commission (contracts 4001, 0011, 05-901, and 1001 to the Arizona Parkinson-s Disease Consortium) and the Michael J. Fox Foundation for Parkinson's Research.

The mouse strain used for this research project, B6SJL-Tg(APPSwFlLon, PSEN1*M146L *L286V)6799Vas/Mmjax, RRID:MMRRC_034840-JAX, was obtained from the Mutant Mouse Resource and Research Center (MMRRC) at The Jackson Laboratory, an NIH-funded strain repository, and was donated to the MMRRC by Robert Vassar, Ph.D., Northwestern University.

Funding Support

This work was supported by the National Institutes of Health (R00 HL140106, R01 AG073230 to PWP), the Alzheimer's Association (AARGD-21-850835 to PWP), and the Arizona Alzheimer's Consortium, Arizona Department of Health Services.

Conflict of interest

The authors declare no conflicts of interest.

Supplemental Material

A detailed description of the materials and methods is provided in the *Supplemental Material.*

Author Contribution

JFS – conceived, designed, performed the experiments, analyzed data, and wrote the initial draft of the manuscript;

FDP – performed experiments and analyzed data;

PM – performed experiments and analyzed data;

SHT – performed experiments and analyzed data;

ECL – performed experiments and analyzed data;

463 **AS** – performed the experiments and analyzed data;

464 **AMK** – performed experiments and analyzed data;

465 **MTG** – performed the experiments and analyzed data;

466 **PWP** – conceived, designed, performed experiments, analyzed data and revised the draft of the
467 manuscript.

468 All authors declare that they reviewed and edited the manuscript, and agree to its submission.

469

470

471 **References**

472 1. 2021 Alzheimer's disease facts and figures. *Alzheimers Dement*. 2021;17:327-406. doi:
473 10.1002/alz.12328
474 2. Girard SD, Baranger K, Gauthier C, Jacquet M, Bernard A, Escoffier G, Marchetti E,
475 Khrestchatisky M, Rivera S, Roman FS. Evidence for early cognitive impairment related
476 to frontal cortex in the 5XFAD mouse model of Alzheimer's disease. *J Alzheimers Dis*.
477 2013;33:781-796. doi: 10.3233/JAD-2012-120982
478 3. Collaborators GBDDF. Estimation of the global prevalence of dementia in 2019 and
479 forecasted prevalence in 2050: an analysis for the Global Burden of Disease Study 2019.
480 *Lancet Public Health*. 2022;7:e105-e125. doi: 10.1016/S2468-2667(21)00249-8
481 4. Jellinger KA. Alzheimer disease and cerebrovascular pathology: an update. *J Neural*
482 *Transm (Vienna)*. 2002;109:813-836. doi: 10.1007/s007020200068
483 5. Mehndiratta P, Manjila S, Ostergard T, Eisele S, Cohen ML, Sila C, Selman WR. Cerebral
484 amyloid angiopathy-associated intracerebral hemorrhage: pathology and management.
485 *Neurosurg Focus*. 2012;32:E7. doi: 10.3171/2012.1.FOCUS11370
486 6. Gireud-Goss M, Mack AF, McCullough LD, Urayama A. Cerebral Amyloid Angiopathy and
487 Blood-Brain Barrier Dysfunction. *Neuroscientist*. 2021;27:668-684. doi:
488 10.1177/1073858420954811
489 7. Greenberg SM, Gurol ME, Rosand J, Smith EE. Amyloid angiopathy-related vascular
490 cognitive impairment. *Stroke*. 2004;35:2616-2619. doi:
491 10.1161/01.STR.0000143224.36527.44
492 8. Shin HK, Jones PB, Garcia-Alloza M, Borrelli L, Greenberg SM, Bacskai BJ, Frosch MP,
493 Hyman BT, Moskowitz MA, Ayata C. Age-dependent cerebrovascular dysfunction in a
494 transgenic mouse model of cerebral amyloid angiopathy. *Brain*. 2007;130:2310-2319. doi:
495 10.1093/brain/awm156
496 9. Iadecola C. The Neurovascular Unit Coming of Age: A Journey through Neurovascular
497 Coupling in Health and Disease. *Neuron*. 2017;96:17-42. doi:
498 10.1016/j.neuron.2017.07.030
499 10. Nelson MT, Quayle JM. Physiological roles and properties of potassium channels in
500 arterial smooth muscle. *Am J Physiol*. 1995;268:C799-822. doi:
501 10.1152/ajpcell.1995.268.4.C799
502 11. Brenner R, Perez GJ, Bonev AD, Eckman DM, Kosek JC, Wiler SW, Patterson AJ, Nelson
503 MT, Aldrich RW. Vasoregulation by the beta1 subunit of the calcium-activated potassium
504 channel. *Nature*. 2000;407:870-876. doi: 10.1038/35038011

505 12. Jaggar JH, Porter VA, Lederer WJ, Nelson MT. Calcium sparks in smooth muscle. *Am J*
506 *Physiol Cell Physiol*. 2000;278:C235-256. doi: 10.1152/ajpcell.2000.278.2.C235
507 13. Krishnamoorthy-Natarajan G, Koide M. BK Channels in the Vascular System. *Int Rev*
508 *Neurobiol*. 2016;128:401-438. doi: 10.1016/bs.irn.2016.03.017
509 14. Tian L, Jeffries O, McClafferty H, Molyvdas A, Rowe IC, Saleem F, Chen L, Greaves J,
510 Chamberlain LH, Knaus HG, et al. Palmitoylation gates phosphorylation-dependent
511 regulation of BK potassium channels. *Proc Natl Acad Sci U S A*. 2008;105:21006-21011.
512 doi: 10.1073/pnas.0806700106
513 15. Schubert R, Nelson MT. Protein kinases: tuners of the BKCa channel in smooth muscle.
514 *Trends Pharmacol Sci*. 2001;22:505-512. doi: 10.1016/s0165-6147(00)01775-2
515 16. Kyle BD, Braun AP. The regulation of BK channel activity by pre- and post-translational
516 modifications. *Front Physiol*. 2014;5:316. doi: 10.3389/fphys.2014.00316
517 17. Thuringer D, Findlay I. Contrasting effects of intracellular redox couples on the regulation
518 of maxi-K channels in isolated myocytes from rabbit pulmonary artery. *J Physiol*. 1997;500
519 (Pt 3):583-592. doi: 10.1113/jphysiol.1997.sp022044
520 18. Lang RJ, Harvey JR, McPhee GJ, Klemm MF. Nitric oxide and thiol reagent modulation of
521 Ca2+-activated K+ (BKCa) channels in myocytes of the guinea-pig taenia caeci. *J Physiol*.
522 2000;525 Pt 2:363-376. doi: 10.1111/j.1469-7793.2000.00363.x
523 19. Brzezinska AK, Gebremedhin D, Chilian WM, Kalyanaraman B, Elliott SJ. Peroxynitrite
524 reversibly inhibits Ca(2+)-activated K(+) channels in rat cerebral artery smooth muscle
525 cells. *Am J Physiol Heart Circ Physiol*. 2000;278:H1883-1890. doi:
526 10.1152/ajpheart.2000.278.6.H1883
527 20. Wang ZW, Nara M, Wang YX, Kotlikoff MI. Redox regulation of large conductance Ca(2+)-
528 activated K+ channels in smooth muscle cells. *J Gen Physiol*. 1997;110:35-44. doi:
529 10.1085/jgp.110.1.35
530 21. Soto MA, Gonzalez C, Lissi E, Vergara C, Latorre R. Ca(2+)-activated K+ channel
531 inhibition by reactive oxygen species. *Am J Physiol Cell Physiol*. 2002;282:C461-471. doi:
532 10.1152/ajpcell.00167.2001
533 22. Furuta S. Basal S-Nitrosylation Is the Guardian of Tissue Homeostasis. *Trends Cancer*.
534 2017;3:744-748. doi: 10.1016/j.trecan.2017.09.003
535 23. Butterfield DA, Boyd-Kimball D. Mitochondrial Oxidative and Nitrosative Stress and
536 Alzheimer Disease. *Antioxidants (Basel)*. 2020;9. doi: 10.3390/antiox9090818

537 24. Handy DE, Loscalzo J. Nitric oxide and posttranslational modification of the vascular
538 proteome: S-nitrosation of reactive thiols. *Arterioscler Thromb Vasc Biol*. 2006;26:1207-
539 1214. doi: 10.1161/01.ATV.0000217632.98717.a0
540 25. Su B, Wang X, Nunomura A, Moreira PI, Lee HG, Perry G, Smith MA, Zhu X. Oxidative
541 stress signaling in Alzheimer's disease. *Curr Alzheimer Res*. 2008;5:525-532. doi:
542 10.2174/156720508786898451
543 26. Asiimwe N, Yeo SG, Kim MS, Jung J, Jeong NY. Nitric Oxide: Exploring the Contextual
544 Link with Alzheimer's Disease. *Oxid Med Cell Longev*. 2016;2016:7205747. doi:
545 10.1155/2016/7205747
546 27. Girouard H, Park L, Anrather J, Zhou P, Iadecola C. Cerebrovascular nitrosative stress
547 mediates neurovascular and endothelial dysfunction induced by angiotensin II.
548 *Arterioscler Thromb Vasc Biol*. 2007;27:303-309. doi:
549 10.1161/01.ATV.0000253885.41509.25
550 28. Taylor JL, Pritchard HAT, Walsh KR, Strangward P, White C, Hill-Eubanks D, Alakrawi M,
551 Hennig GW, Allan SM, Nelson MT, Greenstein AS. Functionally linked potassium channel
552 activity in cerebral endothelial and smooth muscle cells is compromised in Alzheimer's
553 disease. *Proc Natl Acad Sci U S A*. 2022;119:e2204581119. doi:
554 10.1073/pnas.2204581119
555 29. Oakley H, Cole SL, Logan S, Maus E, Shao P, Craft J, Guillozet-Bongaarts A, Ohno M,
556 Disterhoft J, Van Eldik L, et al. Intraneuronal beta-amyloid aggregates,
557 neurodegeneration, and neuron loss in transgenic mice with five familial Alzheimer's
558 disease mutations: potential factors in amyloid plaque formation. *J Neurosci*.
559 2006;26:10129-10140. doi: 10.1523/JNEUROSCI.1202-06.2006
560 30. 2022 Alzheimer's disease facts and figures. *Alzheimers Dement*. 2022;18:700-789. doi:
561 10.1002/alz.12638
562 31. Peters EC, Gee MT, Pawlowski LN, Kath AM, Polk FD, Vance CJ, Sacoman JL, Pires PW.
563 Amyloid-beta disrupts unitary calcium entry through endothelial NMDA receptors in mouse
564 cerebral arteries. *Journal of cerebral blood flow and metabolism : official journal of the*
565 *International Society of Cerebral Blood Flow and Metabolism*. 2022;42:145-161. doi:
566 10.1177/0271678X211039592
567 32. Jackson WF. Myogenic Tone in Peripheral Resistance Arteries and Arterioles: The
568 Pressure Is On! *Front Physiol*. 2021;12:699517. doi: 10.3389/fphys.2021.699517

569 33. Newcombe EA, Camats-Perna J, Silva ML, Valmas N, Huat TJ, Medeiros R. Inflammation:
570 the link between comorbidities, genetics, and Alzheimer's disease. *J Neuroinflammation*.
571 2018;15:276. doi: 10.1186/s12974-018-1313-3
572 34. Cinelli MA, Do HT, Miley GP, Silverman RB. Inducible nitric oxide synthase: Regulation,
573 structure, and inhibition. *Med Res Rev*. 2020;40:158-189. doi: 10.1002/med.21599
574 35. Kleinert H, Schwarz PM, Forstermann U. Regulation of the expression of inducible nitric
575 oxide synthase. *Biol Chem*. 2003;384:1343-1364. doi: 10.1515/BC.2003.152
576 36. Forstermann U, Xia N, Li H. Roles of Vascular Oxidative Stress and Nitric Oxide in the
577 Pathogenesis of Atherosclerosis. *Circ Res*. 2017;120:713-735. doi:
578 10.1161/CIRCRESAHA.116.309326
579 37. Weidinger A, Mullebner A, Paier-Pourani J, Banerjee A, Miller I, Lauterbock L, Duvigneau
580 JC, Skulachev VP, Redl H, Kozlov AV. Vicious inducible nitric oxide synthase-
581 mitochondrial reactive oxygen species cycle accelerates inflammatory response and
582 causes liver injury in rats. *Antioxid Redox Signal*. 2015;22:572-586. doi:
583 10.1089/ars.2014.5996
584 38. Viner RI, Williams TD, Schoneich C. Peroxynitrite modification of protein thiols: oxidation,
585 nitrosylation, and S-glutathiolation of functionally important cysteine residue(s) in the
586 sarcoplasmic reticulum Ca-ATPase. *Biochemistry*. 1999;38:12408-12415. doi:
587 10.1021/bi9909445
588 39. Newell KL, Hyman BT, Growdon JH, Hedley-Whyte ET. Application of the National
589 Institute on Aging (NIA)-Reagan Institute criteria for the neuropathological diagnosis of
590 Alzheimer disease. *J Neuropathol Exp Neurol*. 1999;58:1147-1155. doi:
591 10.1097/00005072-199911000-00004
592 40. Polycarpou A, Hricisak L, Iring A, Safar D, Ruisanchez E, Horvath B, Sandor P, Benyo Z.
593 Adaptation of the cerebrocortical circulation to carotid artery occlusion involves blood flow
594 redistribution between cortical regions and is independent of eNOS. *Am J Physiol Heart*
595 *Circ Physiol*. 2016;311:H972-H980. doi: 10.1152/ajpheart.00197.2016
596 41. Blackwell JA, Silva JF, Louis EM, Savu A, Largent-Milnes TM, Brooks HL, Pires PW.
597 Cerebral arteriolar and neurovascular dysfunction after chemically induced menopause in
598 mice. *Am J Physiol Heart Circ Physiol*. 2022;323:H845-H860. doi:
599 10.1152/ajpheart.00276.2022
600 42. Breijyeh Z, Karaman R. Comprehensive Review on Alzheimer's Disease: Causes and
601 Treatment. *Molecules*. 2020;25. doi: 10.3390/molecules25245789

602 43. Bryant A, Li Z, Jayakumar R, Serrano-Pozo A, Woost B, Hu M, Woodbury ME, Wachter
603 A, Lin G, Kwon T, et al. Endothelial Cells Are Heterogeneous in Different Brain Regions
604 and Are Dramatically Altered in Alzheimer's Disease. *J Neurosci*. 2023;43:4541-4557. doi:
605 10.1523/JNEUROSCI.0237-23.2023
606 44. Andjelkovic AV, Situ M, Citalan-Madrid AF, Stamatovic SM, Xiang J, Keep RF. Blood-
607 Brain Barrier Dysfunction in Normal Aging and Neurodegeneration: Mechanisms, Impact,
608 and Treatments. *Stroke*. 2023;54:661-672. doi: 10.1161/STROKEAHA.122.040578
609 45. Scheuermann BC, Parr SK, Schulze KM, Kunkel ON, Turpin VG, Liang J, Ade CJ.
610 Associations of Cerebrovascular Regulation and Arterial Stiffness With Cerebral Small
611 Vessel Disease: A Systematic Review and Meta-Analysis. *J Am Heart Assoc*.
612 2023;12:e032616. doi: 10.1161/JAHA.123.032616
613 46. Niwa K, Kazama K, Younkin L, Younkin SG, Carlson GA, Iadecola C. Cerebrovascular
614 autoregulation is profoundly impaired in mice overexpressing amyloid precursor protein.
615 *Am J Physiol Heart Circ Physiol*. 2002;283:H315-323. doi: 10.1152/ajpheart.00022.2002
616 47. Heutz R, Claassen J, Feiner S, Davies A, Gurung D, Panerai RB, Heus R, Beishon LC.
617 Dynamic cerebral autoregulation in Alzheimer's disease and mild cognitive impairment: A
618 systematic review. *Journal of cerebral blood flow and metabolism : official journal of the*
619 *International Society of Cerebral Blood Flow and Metabolism*. 2023;43:1223-1236. doi:
620 10.1177/0271678X231173449
621 48. Nieves-Cintron M, Syed AU, Buonarati OR, Rigor RR, Nystoriak MA, Ghosh D, Sasse KC,
622 Ward SM, Santana LF, Hell JW, Navedo MF. Impaired BK(Ca) channel function in native
623 vascular smooth muscle from humans with type 2 diabetes. *Sci Rep*. 2017;7:14058. doi:
624 10.1038/s41598-017-14565-9
625 49. Lu T, Chai Q, Jiao G, Wang XL, Sun X, Furuseth JD, Stulak JM, Daly RC, Greason KL,
626 Cha YM, Lee HC. Downregulation of BK channel function and protein expression in
627 coronary arteriolar smooth muscle cells of type 2 diabetic patients. *Cardiovasc Res*.
628 2019;115:145-153. doi: 10.1093/cvr/cvy137
629 50. Grimm PR, Sansom SC. BK channels and a new form of hypertension. *Kidney Int*.
630 2010;78:956-962. doi: 10.1038/ki.2010.272
631 51. Taylor JL, Walsh KR, Mosneag IE, Danby TGE, Luka N, Chanda B, Schiessl I, Dunne RA,
632 Hill-Eubanks D, Hennig GW, et al. Uncoupling of Ca(2+) sparks from BK channels in
633 cerebral arteries underlies hypoperfusion in hypertension-induced vascular dementia.
634 *Proc Natl Acad Sci U S A*. 2023;120:e2307513120. doi: 10.1073/pnas.2307513120

635 52. Reed JT, Pareek T, Sriramula S, Pabbidi MR. Aging influences cerebrovascular myogenic
636 reactivity and BK channel function in a sex-specific manner. *Cardiovasc Res*.
637 2020;116:1372-1385. doi: 10.1093/cvr/cvz314
638 53. Le T, Martin-Aragon Baudel M, Syed A, Singhrao N, Pan S, Flores-Tamez VA, Burns AE,
639 Man KNM, Karey E, Hong J, et al. Secondhand Smoke Exposure Impairs Ion Channel
640 Function and Contractility of Mesenteric Arteries. *Function (Oxf)*. 2021;2:zqab041. doi:
641 10.1093/function/zqab041
642 54. Liu YP, Zhang TN, Wen R, Liu CF, Yang N. Role of Posttranslational Modifications of
643 Proteins in Cardiovascular Disease. *Oxid Med Cell Longev*. 2022;2022:3137329. doi:
644 10.1155/2022/3137329
645 55. Bolotina VM, Najibi S, Palacino JJ, Pagano PJ, Cohen RA. Nitric oxide directly activates
646 calcium-dependent potassium channels in vascular smooth muscle. *Nature*.
647 1994;368:850-853. doi: 10.1038/368850a0
648 56. Hou S, Heinemann SH, Hoshi T. Modulation of BKCa channel gating by endogenous
649 signaling molecules. *Physiology (Bethesda)*. 2009;24:26-35. doi:
650 10.1152/physiol.00032.2008
651 57. Hou S, Xu R, Heinemann SH, Hoshi T. The RCK1 high-affinity Ca2+ sensor confers
652 carbon monoxide sensitivity to Slo1 BK channels. *Proc Natl Acad Sci U S A*.
653 2008;105:4039-4043. doi: 10.1073/pnas.0800304105
654 58. Liu Y, Terata K, Chai Q, Li H, Kleinman LH, Gutterman DD. Peroxynitrite inhibits Ca2+-
655 activated K+ channel activity in smooth muscle of human coronary arterioles. *Circ Res*.
656 2002;91:1070-1076. doi: 10.1161/01.res.0000046003.14031.98
657 59. Kinney JW, Bemiller SM, Murtishaw AS, Leisgang AM, Salazar AM, Lamb BT.
658 Inflammation as a central mechanism in Alzheimer's disease. *Alzheimers Dement (N Y)*.
659 2018;4:575-590. doi: 10.1016/j.trci.2018.06.014
660 60. Venema RC, Sayegh HS, Kent JD, Harrison DG. Identification, characterization, and
661 comparison of the calmodulin-binding domains of the endothelial and inducible nitric oxide
662 synthases. *J Biol Chem*. 1996;271:6435-6440. doi: 10.1074/jbc.271.11.6435
663 61. Filosa JA, Bonev AD, Straub SV, Meredith AL, Wilkerson MK, Aldrich RW, Nelson MT.
664 Local potassium signaling couples neuronal activity to vasodilation in the brain. *Nat*
665 *Neurosci*. 2006;9:1397-1403. doi: 10.1038/nn1779
666 62. Pritchard HAT, Pires PW, Yamasaki E, Thakore P, Earley S. Nanoscale remodeling of
667 ryanodine receptor cluster size underlies cerebral microvascular dysfunction in Duchenne
668 muscular dystrophy. *Proc Natl Acad Sci U S A*. 2018. doi: 10.1073/pnas.1804593115

669 63. Dennison JL, Ricciardi NR, Lohse I, Volmar CH, Wahlestedt C. Sexual Dimorphism in the
670 3xTg-AD Mouse Model and Its Impact on Pre-Clinical Research. *J Alzheimers Dis*.
671 2021;80:41-52. doi: 10.3233/JAD-201014
672 64. Toro CA, Zhang L, Cao J, Cai D. Sex differences in Alzheimer's disease: Understanding
673 the molecular impact. *Brain Res*. 2019;1719:194-207. doi: 10.1016/j.brainres.2019.05.031
674 65. Prange-Kiel J, Dudzinski DA, Prols F, Glatzel M, Matschke J, Rune GM. Aromatase
675 Expression in the Hippocampus of AD Patients and 5xFAD Mice. *Neural Plast*.
676 2016;2016:9802086. doi: 10.1155/2016/9802086
677 66. Arias-Loza PA, Muehlfelder M, Pelzer T. Estrogen and estrogen receptors in
678 cardiovascular oxidative stress. *Pflugers Arch*. 2013;465:739-746. doi: 10.1007/s00424-
679 013-1247-7
680 67. Tran QK. Reciprocality Between Estrogen Biology and Calcium Signaling in the
681 Cardiovascular System. *Front Endocrinol (Lausanne)*. 2020;11:568203. doi:
682 10.3389/fendo.2020.568203
683 68. Cheng YJ, Lin CH, Lane HY. From Menopause to Neurodegeneration-Molecular Basis
684 and Potential Therapy. *Int J Mol Sci*. 2021;22. doi: 10.3390/ijms22168654
685 69. Razmara A, Duckles SP, Krause DN, Procaccio V. Estrogen suppresses brain
686 mitochondrial oxidative stress in female and male rats. *Brain Res*. 2007;1176:71-81. doi:
687 10.1016/j.brainres.2007.08.036
688 70. Gadomsky L, Dos Santos Guilherme M, Winkler J, van der Kooij MA, Hartmann T, Grimm
689 M, Endres K. Elevated Testosterone Level and Urine Scent Marking in Male 5xFAD
690 Alzheimer Model Mice. *Curr Alzheimer Res*. 2020;17:80-92. doi:
691 10.2174/1567205017666200217105537

692

693

694 **Figure Legends**

695 **Figure 1.** *Cerebral microvascular hyper-contractility in 5x-FAD*. **A,E)** Representative traces of the
696 lumen diameter of pial arteries isolated from female (**A**) and male (**E**) WT (black, top) or *5x-FAD*
697 (lower, red) during the generation of spontaneous myogenic tone. Arrows indicate the moment
698 when intraluminal pressure was raised from 15 to 50 mmHg. **B, F)** Summary data showing higher
699 spontaneous myogenic tone in pial arteries from female (**B**) and male (**F**) *5x-FAD*. **C, G)** Pial
700 artery contractility to endothelin-1 (ET-1) was significantly increased in female (**C**) and male (**G**)
701 *5x-FAD* when compared to WT littermates. **D, H)** Receptor-independent contraction to a
702 depolarizing stimulus (60 mM KCl) was unchanged in female (**D**) and male (**H**). All data are means
703 ± SEM. Each data point in graphs represents 1 pial artery from 1 mouse. Statistical analysis:
704 unpaired two-tailed Mann-Whitney (**B, F**) or unpaired two-tailed *Student*'s t-test (**C, D, G, H**).

705 **Figure 2.** *BK_{Ca} impairment in pial arteries from 5x-FAD.* **A, E)** Representative traces of the lumen
706 diameter of pial arteries isolated from female (**A**) and male (**E**) WT (black, top) or *5x-FAD* (lower,
707 red) showing constriction to the BK_{Ca} blocker iberiotoxin (IbTox, 30 nM). Note the blunted
708 constriction in *5x-FAD* mice. Orange boxes: regions where data were obtained**. B, F)** Summary
709 bar graph showing blunted vasoconstriction to IbTox in female (**B**) and male (**F**) *5x-FAD*. Each
710 data point in the graph represents 1 pial artery from 1 mouse. Statistical test: unpaired two-tailed
711 Mann-Whitney test. **C, G)** Representative traces of an inside-out patch clamp from freshly-isolated
712 pial artery smooth muscle cells showing single channel BK_{Ca} currents at a holding potential of +60
713 mV. Note the higher frequency of openings (downward deflections) in the patch from female (**C**)
714 WT (top trace, black) compared to *5x-FAD* (lower trace, red). Single channel BK_{Ca} openings were
715 not different between males WT and *5x-FAD* (**G**). C: closed; 1: 1 channel; 2: 2 channels. **D, H)**
716 Summary graph showing BK_{Ca} open probability (Po) over a range of holding potentials (+20, +40,
717 +60 mV). Po was significantly lower in inside-out patches from pial artery smooth muscle cells
718 isolated from female *5x-FAD* mice (**D**), whereas BK_{Ca} Po was not different between males *5x-*
719 *FAD* and WT littermates (**H**). Number of female replicates: WT n = 10 patches from 5 different
720 mice; *5x-FAD* n = 7 patches from 4 different mice. Number of male replicates: WT n = 9 patches
721 from 5 different mice; *5x-FAD* n = 9 patches from 6 different mice. All data are means ± SEM,
722 two-way ANOVA with a Sidak *post-hoc* test.

723 **Figure 3.** *BK_{Ca} impairment in males is a consequence of lower BK_{α} expression and reduced Ca^{2+}*
724 *sparks activity.* **A-B)** Expression levels of BK_{α} mRNA (**A**) and protein (**B**) are not different between
725 female *5x-FAD* and WT littermates. WB: Western blot. Each data point in the graph is a pial artery
726 lysate from 1 mouse. Statistical analysis: unpaired two-tailed *Student*'s t-test. **C-D**) Expression

727 levels of BK_{α} mRNA are similar between male *5x-FAD* and WT littermates (**C**); however BK_{α}
728 protein expression is significantly lower in male *5x-FAD* when compared to WT littermates (**D**).
729 Each data point in the graph is a pial artery lysate from 1 mouse. Statistical analysis: unpaired
730 two-tailed *Student*'s t-test. **E-J)** Representative greyscale (**Ei, Fi**) and pseudocolored (**Eii, Fii**)
731 images of fields of view of pial arteries from female WT (**E**) and *5x-FAD* (**F**) prepared *reverse en*
732 face for recording of Ca^{2+} sparks (arrows). Ca^{2+} sparks frequency (**I**) was significantly higher in
733 pial arteries from female *5x-FAD* than in WT littermates, without differences in the number of
734 active sites per cell (**J**). Each data point in the graph is 1 field of view from a pial artery, for a total
735 of 5 fields of view per artery from 3 different mice of each genotype. Statistical analysis: unpaired
736 two-tailed *Student*'s t-test. **G-L)** Representative greyscale (**Gi, Hi**) and pseudocolored (**Gii, Hii**)
737 images of fields of view of pial arteries from male WT (**G**) and *5x-FAD* (**H**) prepared *reverse en*
738 face for recording of Ca^{2+} sparks (arrows). Ca^{2+} sparks frequency (**K**) was significantly lower in
739 pial arteries from male *5x-FAD* than in WT littermates, without differences in the number of active
740 sites per cell (**L**). Each data point in the graph is 1 field of view from a pial artery, for a total of 5
741 fields of view per artery from 3 different mice of each genotype. Statistical analysis: unpaired two-
742 tailed *Student*'s t-test. All data are means ± SEM.

743

744 **Figure 4**. *Oxidative-dependent BK_{Ca} impairment in pial arteries from female 5x-FAD.* **A-C)**
745 Glutathione assay from brain lysates of female *5x-FAD* showing the presence of an oxidative
746 environment, observed as a significant increase in oxidized glutathione (GSSG, **B**) and the ratio
747 between GSSG and reduced glutathione (GSH, **C**). Each data point represents a brain lysate
748 from the cortex of an individual mouse. Statistical analysis: unpaired two-tailed Student's t-test.
749 D-E) Incubation of pial arteries from isolated female *5x-FAD* with the broad-spectrum reducing
750 agent dithiothreitol (DTT, 10 μM) significantly recovers sensitivity to iberiotoxin (30 nM), as
751 observed by the representative trace (**D**) and summary data (**E**). Orange boxes indicate the
752 regions where data were extracted. Each data point in the graph represents 1 pial artery from an
753 individual mouse. Statistical analysis: paired two-tailed *Student*'s t-test. **F-G)** Similarly, acute
754 incubation with DTT partially recovers BK_{Ca} Po in freshly-isolated pial artery smooth muscle cell
755 from female *5x-FAD*, as observed in the representative traces (**F**) and summary data (**G**). N = 16
756 patches from 6 different mice. Statistical analysis: Matching Mixed-Model Anova with a Sidak
757 *post-hoc* correction for multiple comparisons. All data are means ± SEM.

758 **Figure 5**. *Exacerbated BK_{Ca} S-NO in female 5x-FAD.* **A)** Higher iNOS mRNA expression in
759 lysates of pial arteries isolated from female *5x-FAD* than in WT littermates. Each data point

760 represents 1 pial artery lysate from an individual mouse. Statistical analysis: unpaired two-tailed
761 *Student*'s t-test. B) Immunofluorescence labeling of iNOS (red) in pial arteries (collagen IV – Col
762 IV, green). Note the apparent higher fluorescence intensity in iNOS labeling in pial arteries from
763 female *5x-FAD* when compared to WT littermates. Bar = 20 μm. **C)** Blinded, randomized semi-
764 quantitative analysis of iNOS fluorescence intensity in pial arteries of female WT and *5x-FAD*.
765 Each data point represents the average fluorescence intensity of 5 pial arteries randomly imaged
766 from an individual mouse. Statistical analysis: unpaired two-tailed *Student*'s t-test. **D-E)**
767 Quantification of global S-NO proteins in cortical lysates of *5x-FAD* and WT littermates. Note the
768 higher expression of S-NO protein in lysates from *5x-FAD* cortex when compared to WT in the
769 representative blot (**D**) and summary data (**E**). Each data point represents a lysate from an
770 individual mouse. Statistical analysis: unpaired two-tailed Mann-Whitney test. **F-G)** Affinity-
771 purification (AP) of S-NO proteins in brain lysates followed by Western blot against BK_α show a
772 significantly higher expression of BK_α S-NO in female *5x-FAD* when compared to WT littermates,
773 as evidenced by the representative blot (**F**) and summary data (**G**). Each data point represents a
774 lysate from an individual mouse. Statistical analysis: unpaired two-tailed *Studen*t's test. **H-K)** Co-
775 localization analysis using Mander's M1 (**I**) and M2 (**J**) coefficients, as well as the Pearson's
776 coefficient (**K**) show a significantly higher co-localization between of BK_α (**H**, green) and global S-
777 NO proteins (**H**, red) in pial arteries from female *5x-FAD* (fluorogram in **H**) Bar = 20 μm. Violin
778 plots represent the distribution of co-localized pixels in each image. Imaging of pial arteries was
779 performed in a blinded and randomized manner, a total of 3 arteries were imaged per mouse for
780 a total of 5 mice per group. Statistical analysis: unpaired two-tailed Student's t-test. Data in violin
781 plots are median ± 95% confidence intervals, all other data are means ± SEM.

782

783 **Figure 6.** *BK_{Ca} S-NO in post-mortem human brain samples.* **A-B)** Western blot (WB) quantification
784 of BK_α expression in *post-mortem* brain lysates of patients without CAA / AD (Non-AD), CAA or
785 AD + CAA. Representative blots are shown in **A** and summary data in **B**. Each data point
786 represents a brain lysate from an individual age-matched woman (♀) or man (♂). Statistical
787 analysis: Brown-Forsythe and Welch ANOVA with a Dunnett T3 correction for multiple
788 comparisons. **C-D)** Affinity-purification (AP) of S-NO proteins in brain lysates followed by WB
789 against the BK_α subunit show a trend towards an increase in BK_α S-NO in AD + CAA patients
790 when compared to non-AD, as evidenced by the representative blots in **C** and summary data in
791 **D**. Each data point represents a brain lysate from an individual age-matched woman (♀) or man

792 (♂). Statistical analysis: Brown-Forsythe and Welch ANOVA with a Dunnett T3 correction for
793 multiple comparisons. All data are means ± SEM.

794

795 **Figure 7.** *Impaired neurovascular coupling after acute BK_{Ca} inhibition and in 5x-FAD.* **A-C)** Acute
796 application of the BK_{Ca} blocker iberiotoxin (IbTox, 30 nM) atop the thinned-skull cranial window
797 blunted neurovascular responses following somatosensory stimulation in WT mice, as evidenced
798 by the pseudocolored perfusion maps (**A**), representative traces (**B**) of perfusion within the region
799 of interest (black rectangle) and summary data (**C**). Each data point represents an individual
800 mouse, females in square (□) and males in circles (○), after application of vehicle (□, ○) or IbTox
801 (■,●). Statistical analysis: paired two-tailed *Student*'s t-test. **D-I)** Neurovascular coupling
802 responses were significantly impaired in female (**D-F**), and showed a trend towards decrease in
803 male (**G-I**), *5x-FAD* when compared to WT littermates, as evidenced by the perfusion maps (**D,**
804 **G**), representative perfusion traces (**E, H**) and summary data (**F, I**). Each data point represents
805 an individual mouse. Statistical analysis: paired two-tailed *Student*'s t-test. PU = perfusion units.
806 All data are means ± SEM.

Figure 1. *Cerebral microvascular hypercontractility in 5x-FAD*

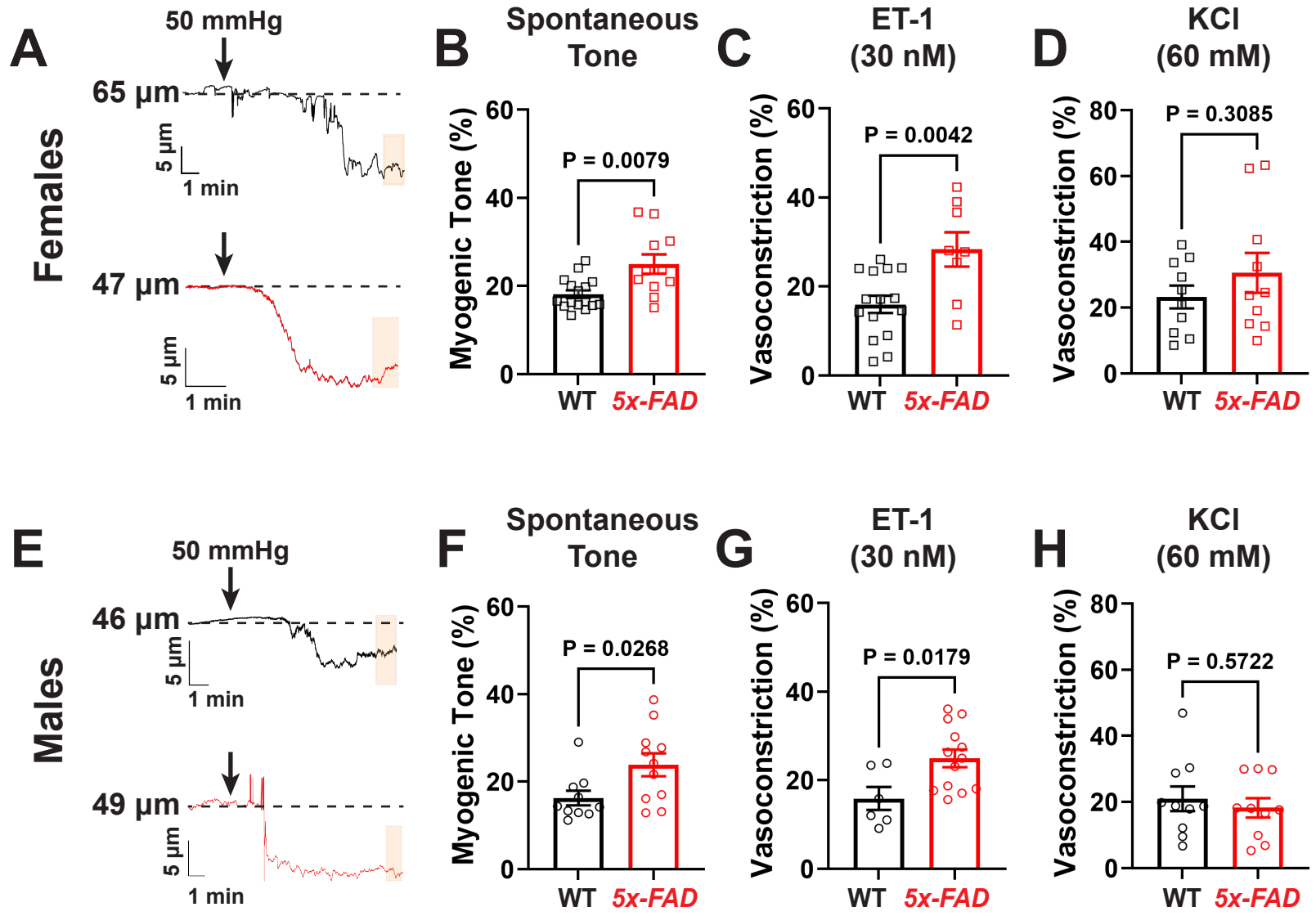

Figure 2. *BK_{Ca} impairment in pial arteries from 5x-FAD*

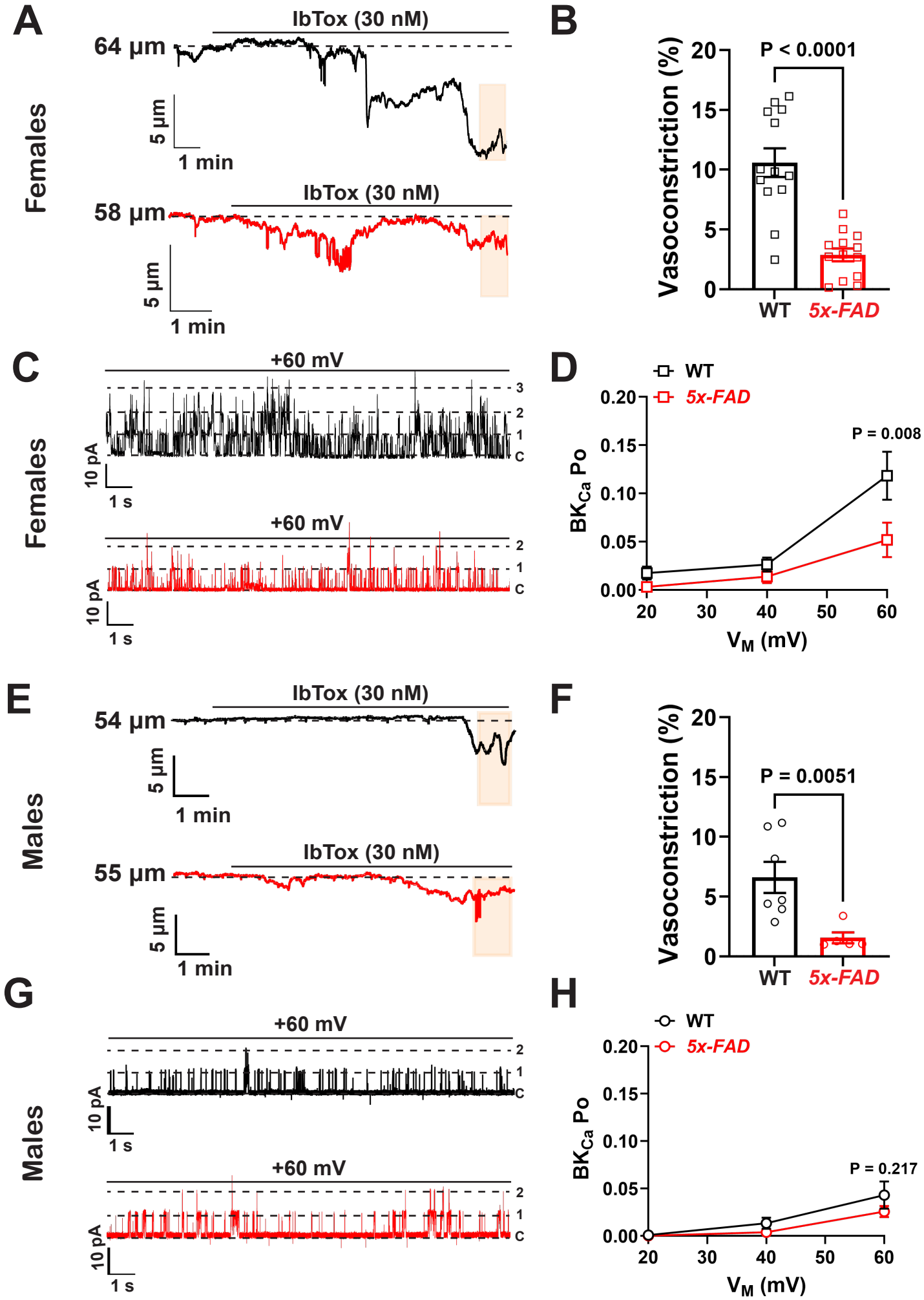

Figure 3. *BK_{Ca} impairment in males is a consequence of lower BK_{α} expression and reduced Ca^{2+} sparks activity.*

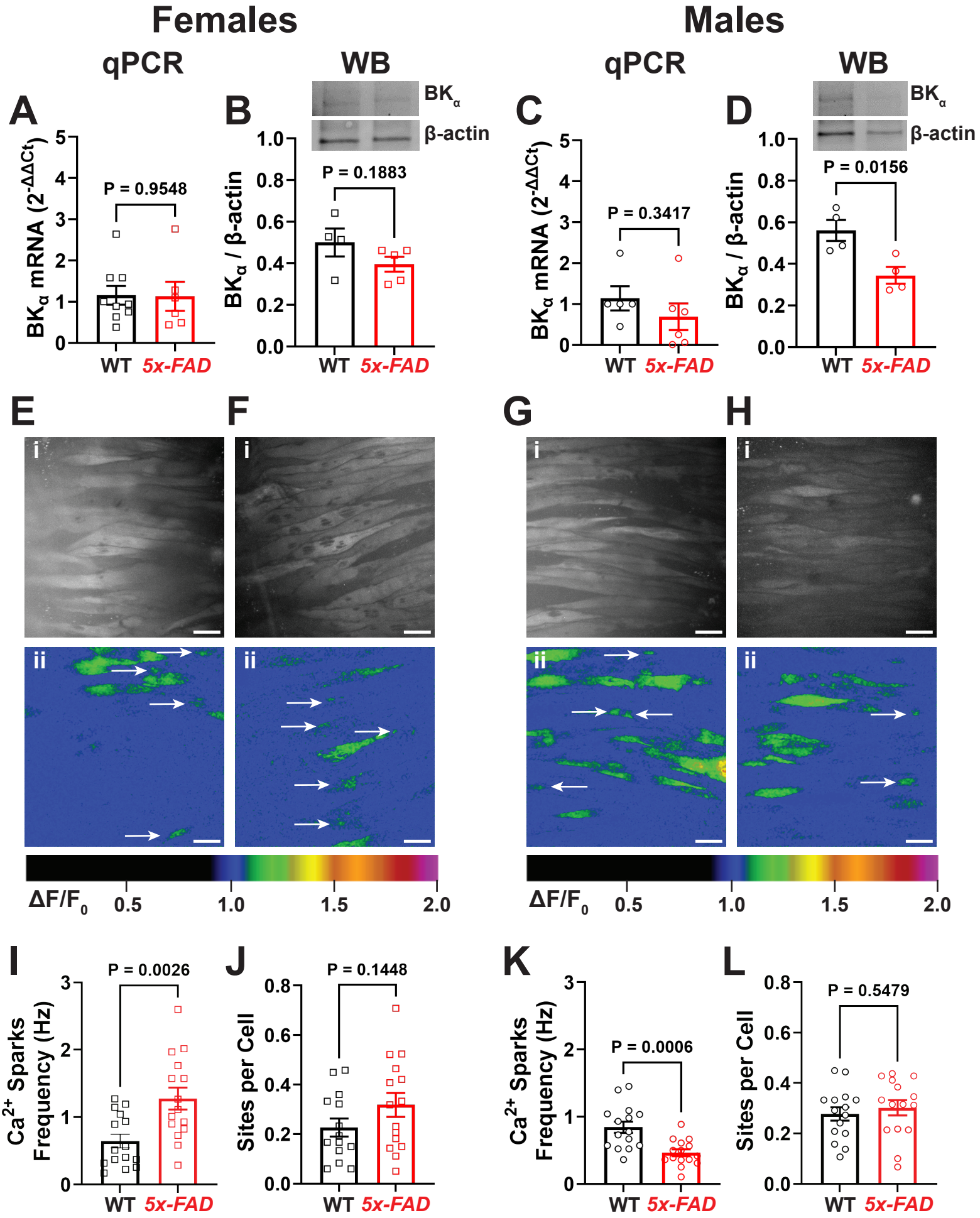

Figure 4. *Oxidative-dependent BK_{Ca} impairment in pial arteries from female 5x-FAD*

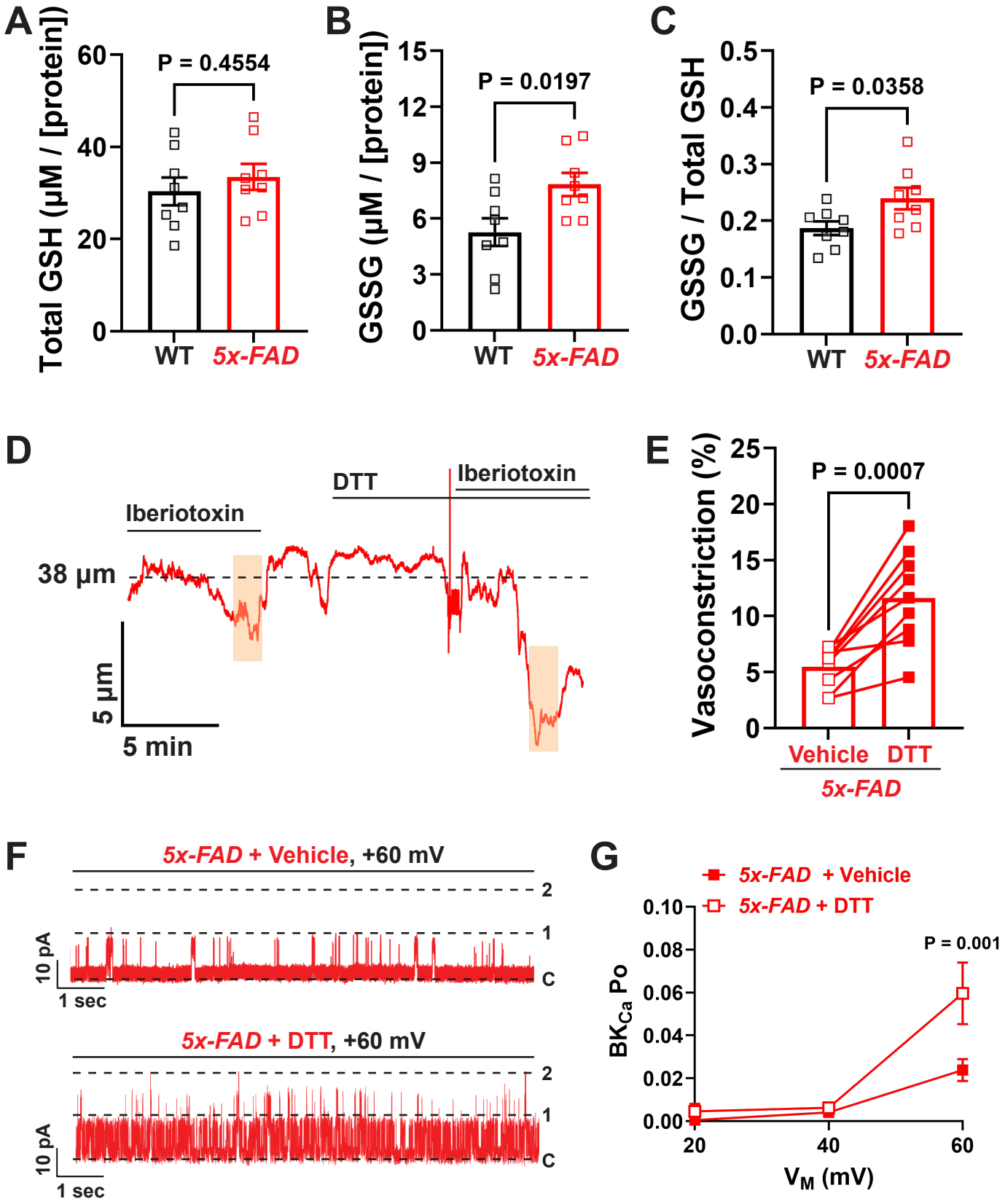

Figure 5. *Exacerbated BK_{Ca} S-NO in female 5x-FAD*

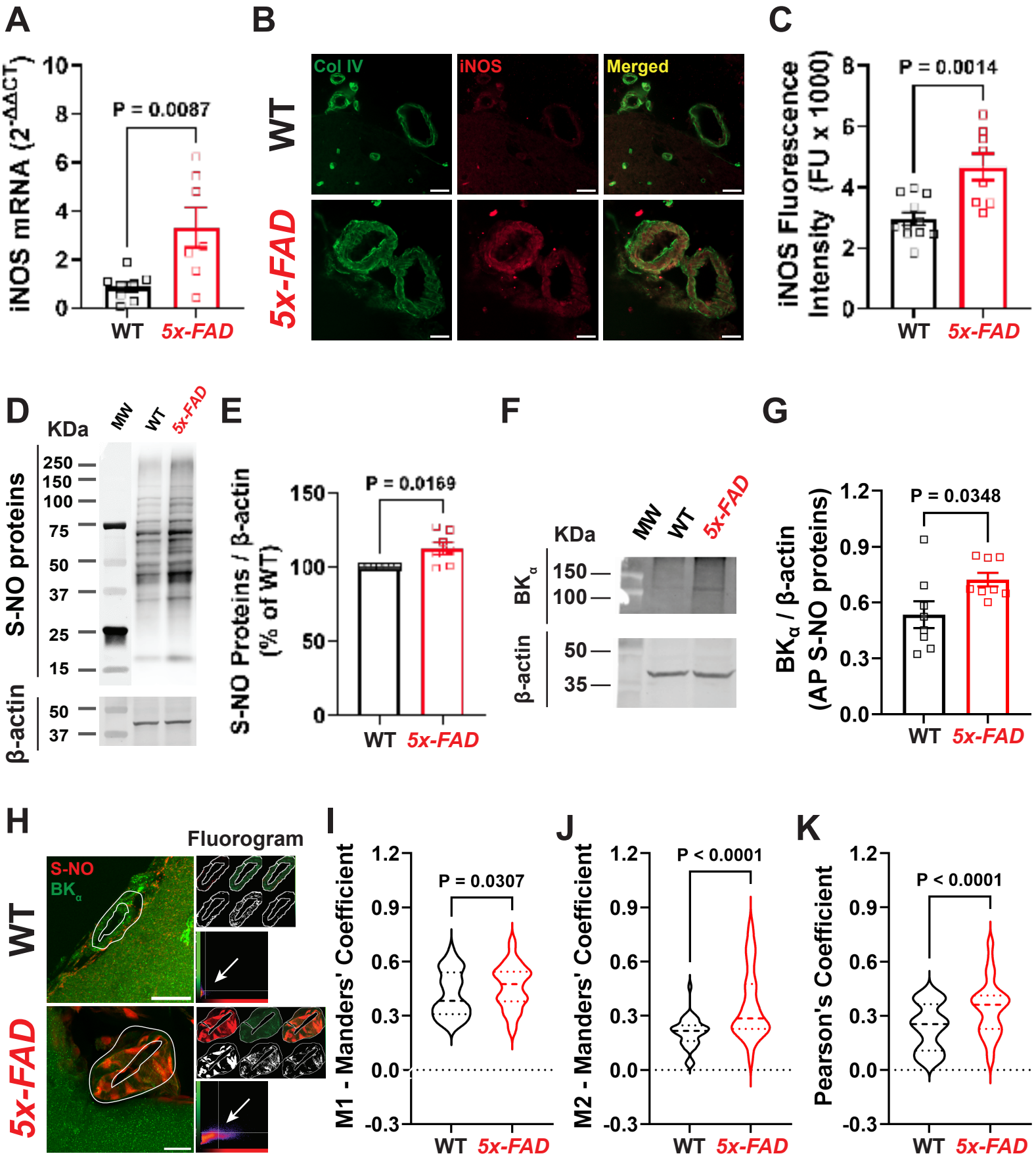

Figure 6. *BK_{Ca} S-NO in post-mortem human brain samples*

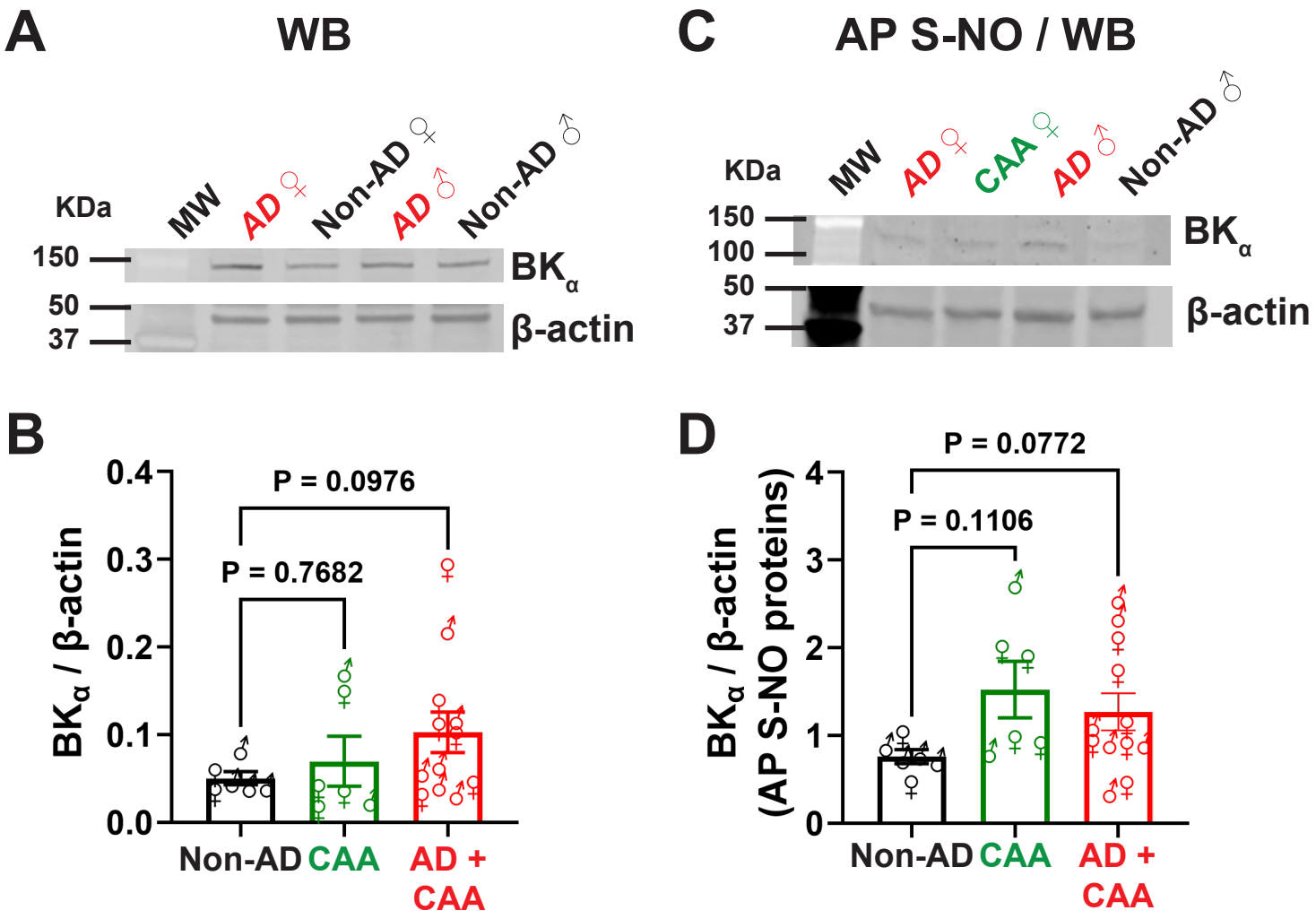
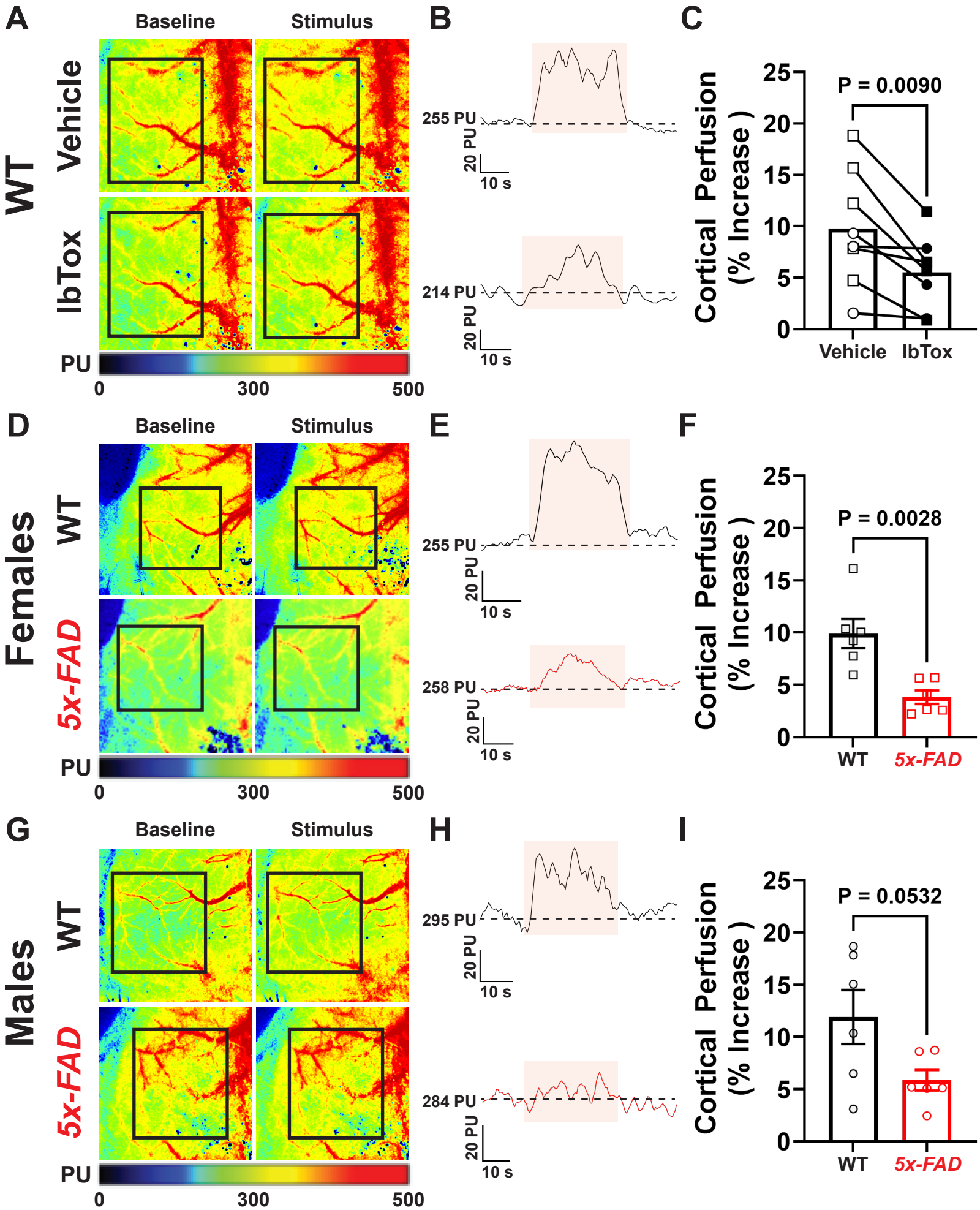
Figure 7. *Impaired neurovascular coupling after acute BK_{Ca} inhibition and in 5x-FAD*